Ripening of surface phases coupled with oscillatory dynamics and self-induced spatial chaos through surface roughening

L. M. Pismen and B. Y. Rubinstein
Department of Chemical Engineering and Minerva Center for Nonlinear Physics of Complex Systems, Technion-Israel Institute of Technology, Technion, Technion City, 32000 Haifa, Israel

(Received 6 August 1998; accepted for publication 3 December 1998)

Some pattern formation processes on single-crystal catalytic surfaces involve transitions between alternative surface phases coupled with oscillatory reaction dynamics. We describe a two-tier symmetry-breaking model of this process, based on nanoscale boundary dynamics interacting with oscillations of adsorbate coverage on microscale. The surface phase distribution oscillates together with adsorbate coverage, and, in addition, undergoes a slow coarsening process due to the curvature dependence of the drift velocity of interphase boundaries. The coarsening is studied both statistically, assuming a circular shape of islands of the minority phase, and through detailed Lagrangian modeling of boundary dynamics. Direct simulation of boundary dynamics allows us to take into account processes of surface reconstruction, leading to self-induced surface roughening. As a result, the surface becomes inhomogeneous, and the coarsening process is arrested way before the thermodynamic limit is reached, leaving a chaotic distribution of surface phases. © *1999 American Institute of Physics.* [S1054-1500(99)01101-5]

Catalytic reactions are often accompanied by structural changes of the surface. These structural changes affect, in their turn, the reaction kinetics. This creates a feedback mechanism leading to complicated spatio-temporal dynamics. In this article we propose a mechanism of pattern formation rooted in interaction between chemical reactions and phase transitions on a catalytic surface, and operating on two widely separated length scales. On the microscopic (nanoscale) level, the competition between surface phases is governed by the local level of rapidly diffusing adsorbed species. On the macroscopic (microscale) level, the balance between alternative states of the surface coverage depends on the area occupied by alternative surface phases. The surface phase distribution oscillates together with adsorbate coverage, and, in addition, undergoes a slow coarsening process due to the curvature dependence of the drift velocity of interphase boundaries. The coarsening is studied both statistically, assuming circular shape of islands of the minority phase, and through detailed modeling of boundary dynamics. A special algorithm developed for direct simulation of boundary dynamics allows to take into account processes of surface reconstruction, leading to self-induced surface roughening. As a result, the surface becomes inhomogeneous, and the system remains ''frozen'' in a state of spatial chaos.

I. INTRODUCTION

Catalytic reactions are often accompanied by deep restructuring of the active surface. This may produce an autocatalytic effect due to enhanced activity of a surface phase formed under reactive conditions. A substantial evidence for this effect has been accumulated in studies of catalytic CO oxidation on single crystal Pt surfaces.[1,2] The mechanism of rate oscillations and pattern formation is based on adsorbate-induced surface phase transitions that are controlled by critical adsorbate coverages, i.e., the $1\times1\rightleftharpoons1\times2$ transition in the case of Pt(110) and the $1\times1\rightleftharpoons$ hex phase transition in the case of Pt(100).[1–4] The phase transition affects the reaction rate mainly through the variation of the oxygen sticking coefficient. In this way, it has been incorporated in the kinetic model of CO oxidation on Pt(110) which includes the fraction of the surface occupied by one of the alternate phases as one of dynamic variables.[5]

Although the model contains three dynamic variables, it turned out to be qualitatively equivalent to a two-variable model, and can be mapped on a standard FitzHugh–Nagumo (FN) system.[6] In a simplified model, the oxygen coverage is slaved to the CO coverage which plays the role of a ''fast activator.'' At a fixed surface phase composition, two alternative stationary states may be attained; one with a high CO coverage that blocks the oxygen access and thereby stifles the reaction, and another with a low CO coverage and higher reaction rate. This bistability phenomenon is common for bimolecular reactions with Langmuir–Hinshelwood kinetics. The domains with prevailing alternative stationary states evolve dynamically due to a relatively slow surface phase transition, so that the surface variable plays the role of a ''slow inhibitor.''

The surface phase transition acts in such a way that the fraction of the 1×1 phase increases on a surface patch with a high CO coverage, leading to an increased O_2 adsorption rate and eventually to a transition to the alternate state, and vice versa. In a lumped system, this leads to relaxation oscillations, and in a spatially extended system, to propagation of surface activity waves, forming either spiral waves, or target patterns, or isolated mobile wave fragments.[1,5,6]

The model by Krischer *et al.* yields a realistic (at least in

a qualitative sense) picture of kinetic oscillations and pattern formation on the Pt(110) surface. Its disadvantage, however, is in a purely phenomenological description of the dynamics of surface reconstruction, using a piecewisely defined function of the CO coverage that insures correct behavior fitting the experimental data. The model also fails to take into account slow changes in catalytic activity which may be caused by surface roughening and faceting.[7–9] These two aspects are in fact related, since surface roughening is likely to occur as a result of repeated transitions between the two surface phases, which, due to their different density of surface atoms, involve a mass transport of Pt atoms.[10] Roughening or faceting might be incorporated into the kinetic model in a natural way if the phase transition could be described more realistically by means of a microscopic model.

A more mechanistic model of this type is the FN-based two-tier symmetry-breaking model[11] that treats the surface phase transition explicitly by replacing the phenomenological equation of the surface variable by a microscale model describing dynamics of domains corresponding to the two surface phases. The essence of the model (Sec. II) is the assumption that the surface phase transition is a slow local process that leads to the formation of a nanoscale pattern of surface phases, and manifests itself in slow motion of interphase boundaries with the speed being dependent on the local value of CO coverage. In turn, the visible (microscale) coverage pattern is determined by average abundance of surface phases within the diffusional range of the adsorbed species.

In this communication, we further elaborate the two-tier model by studying the detailed dynamics of interphase boundaries. This is done on several level of detail. First, we describe the dynamics of distribution of islands of a minority phase taking into account the size dependence of their growth or shrinkage rates. The latter leads to a nonequilibrium analog of Ostwald ripening where the oscillations of the long-range variable act to preserve the abundance of alternative phases averaged over the oscillation period, and thereby imitate a conservation law that commonly keeps the fraction of different phases constant in equilibrium phase transitions. This may lead to growth of average island size up to the characteristic diffusional range of the long-scale variable, thus invalidating the assumptions of both phenomenological[5] and two-tier[11] models.

On the next level (Sec. IV), we carry out detailed modeling of the ripening process with the help of a Lagrangian algorithm based on the local equation of boundary motion. This allows us to describe relaxation of islands to circular shape as well as evolution of size distribution, but leads to qualitatively similar results. The advantage of the detailed model of boundary dynamics justifying a much greater investment of computer resources, is felt, however, when local processes modeling the roughening and faceting of the surface, are incorporated. We further show (Sec. VI) how the local surface modification may be directly correlated in this model with the motion of interphase boundaries. This is done by assuming that surface properties are modified whenever a certain location is passed by the phase transition front. As a result, the ripening process can be arrested by dynamically developing surface inhomogeneities, thus leading to a state of self-induced spatial chaos, and perpetuating the distribution of alternative surface phases intermixed on a fine scale.

II. COARSE-GRAINED TWO-TIER MODEL

A skeleton model capable to give a qualitatively faithful dynamic description of a pattern forming system may operate with the simplest possible nonlinear elements. Rather than considering realistic kinetic equations for the adsorbate coverages, we shall use a single equation for concentration of a fast activator v that can relax to any of two alternate states. We shall also neglect such realistic details as anisotropic diffusion. The simplest suitable evolution equation of v is

$$v_t = \nabla^2 v + (1 - v^2)v - \eta. \tag{1}$$

As in the standard FN model, the two states are biased by the level of the inhibiting variable η, which is defined here in such a way that the level $\eta = 0$ corresponds to the Maxwell construction of the two alternate macrostates. We interpret it here as a surface state variable that models the inhibiting action of the 1×2 reconstruction. In view of the long diffusional range of CO adsorbate (modeled by the activator concentration v), the variable η should be *coarse grained*. It can be interpreted as the *local average* fraction of one of the surface phases computed by spatial averaging over a surface area within the diffusional range of v. The activator acts as a pattern-forming agent on a large scale corresponding to the diffusional range of a mobile adsorbed species (CO). This is the visible pattern observed experimentally on a 10^{-4}–10^{-2} cm scale. The surface variable η, which is slow and nondiffusive, plays the same role of a refractory variable as in the model by Krischer *et al.*[5]

The distinctive feature of the present model lies in designing the evolution equation of the surface variable. On a smaller length scale (in a 10^{-7}–10^{-6} cm range), we conjecture a dynamic pattern of surface phases, consisting of islands of a minority phase immersed in a continuous majority phase. Unlike the phenomenological model,[5] we describe the surface state using a ''microvariable'' u that can relax to two alternate states standing for the surface phases. The dynamics of the microvariable is described by a nonlinear diffusion equation with a cubic nonlinearity,

$$\gamma^{-1} u_t = \delta^2 \nabla^2 u + (1 - u^2)u - \alpha v, \tag{2}$$

where $\delta \ll 1$ is the ratio of the microscopic and macroscopic scales, which is proportional in the physical model to the square root of the ratio of the surface diffusivities of solid (e.g., Pt) atoms and adsorbate. Since the solid diffusivity is small, the borders between the surface phases can be assumed to be almost atomically sharp.

The local value of long-range variable v introduces a bias in favor of one of the surface states. If the coupling parameter α is positive, the lower state advances when the macrovariable v (modeling CO coverage) is positive. The two phases coexist at $\alpha|v| < b = 2/\sqrt{27}$. The speed of the motion (neglecting the curvature effect) is

$$c = \sqrt{6}\,\delta\gamma \sin[\tfrac{1}{3}\arcsin(\tfrac{1}{2}\sqrt{27}\alpha v)] \equiv \delta\gamma\psi(\alpha v). \tag{3}$$

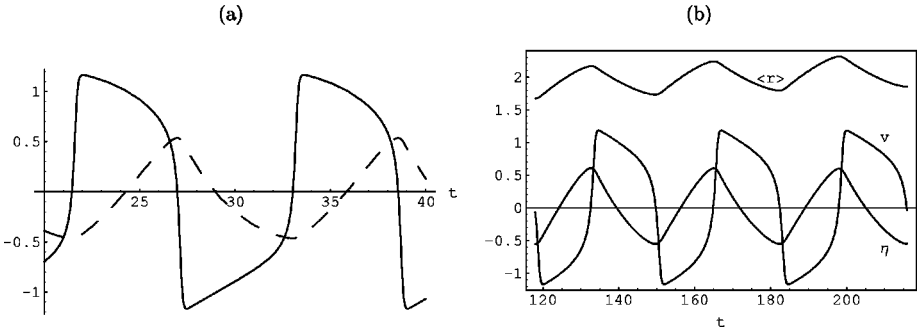

FIG. 1. (a) A typical oscillation cycle at $\gamma \ll 1$; dynamics of v and η are shown by solid and dashed curves, respectively. (b) Short-scale dynamics of the global variable v, the coverage fraction η, and the mean radius ($q=2.43$, $K=0.24$, $\alpha=0.2$).

The dynamics of the surface phases described by this model can be made similar to the dynamics of the surface variable in the phenomenological model of Krischer *et al.*[5] The two values of the CO coverage where the definition of the phenomenological function is changed should correspond to the limits $v=\pm b/\alpha$ of the range of v where the two surface states coexist.

The macrovariable v is affected in turn by the relative abundance of surface phases, described by the coarse-grained variable η. A general relation between η and u can be defined as

$$\eta(x)=\hat{\beta}\left(\int g(x,x')u(x')\,dx'-\hat{s}\right), \tag{4}$$

where $g(x,x')$ is a coarse-graining kernel with a characteristic range of $O(1)$ in the chosen dimensionless units and $\hat{\beta}$, $\hat{s}$ are constants. Assuming sharp interphase borders, η can be directly related to the surface-averaged area covered by the lower surface state $u<0$,

$$\eta(x)=\beta\left(\int g(x,x')H(x')\,dx'-s\right), \tag{5}$$

where $H(x)$ is 1 if the point x is within a domain occupied by the lower state, and 0 otherwise, and β, s are modified constants.

III. OSCILLATIONS AND WAVES

The simplest solution of the coarse-grained equations is obtained by assuming that the diffusional range of the macrovariable v encompasses the entire surface. Under these conditions, v plays the role of a global variable, and obeys Eq. (1) integrated over the entire surface,

$$v_t=(1-v^2)v-\eta. \tag{6}$$

Then the integrals in Eqs. (4) and (5) can be evaluated over the entire surface as well, and the coarse-graining kernel $g(x,x')$ set to unity. If we assume that the lower surface state is a minority phase, and exists in the form of circular islands (sufficiently widely separated, so that their interaction can be neglected), Eq. (5) can be rewritten as

$$\eta=\beta\left(\int f(r)r^2\,dr-s\right)=\beta(n\langle r^2\rangle-s), \tag{7}$$

where $f(r)$ is the instantaneous number density of islands with the radius r, and n is the total number density of islands. The parameter s can be interpreted as the surface fraction corresponding to the Maxwell construction of the two macrostates. This value serves in our model as a bias parameter. Assuming $\beta>0$, negative values of v prevail at $\eta>0$. The multistability range is $|\eta|<b=2/\sqrt{27}$.

For the moment, we neglect the dependence of the boundary speed on the curvature (presuming that the islands are much larger than the diffusional range of the microvariable). Then the change of radii is governed by Eq. (3) which can be transformed by averaging to the evolution equation of η,

$$\frac{d\eta}{dt}=2\beta n\delta\gamma\,\psi(\alpha v)\langle r\rangle(\eta). \tag{8}$$

As long as the dependence of the boundary dynamics on curvature can be neglected, the distribution is shifted rigidly during the oscillation cycle, so that $f(r;t)=f(r+c(\eta)t)$, and, as a consequence, the dispersion $\langle r^2\rangle-\langle r\rangle^2$ remains invariant. This allows to express the mean radius $\langle r\rangle$ through the mean squared radius $\langle r^2\rangle$, which is related to η through Eq. (7). If all islands are of the same size,

$$\langle r\rangle=\sqrt{n^{-1}(s+\eta/\beta)}=\sqrt{s/n(1+\eta/q)}, \tag{9}$$

where $q=\beta s>b$. The final form of Eq. (8) is

$$\frac{d\eta}{dt}=K\psi(\alpha v)\sqrt{1+\eta/q}, \tag{10}$$

where $K=2\beta\delta\gamma\sqrt{sn}$.

A typical picture of relaxation oscillations is obtained at $\gamma\ll 1$. Then the system evolves as follows. If, say, initially $v>0$, the lower state advances and η increases. The macrovariable v continuously adjusts to a changing level of η; it decreases but remains on the upper branch until η reaches the limiting value $\eta=b$. After this, v drops on a fast $O(\gamma)$ time scale to the lower branch. The islands start to shrink, and v grows while η decreases up to the lower critical value $\eta=-b$, after which v jumps back to the upper branch [Fig. 1(a)]; both branches of the oscillation cycle are symmetric.

The above picture is modified if the changing levels of v remove the system from the multistability region of the microvariable or if islands shrink and disappear altogether while the system evolves along the branch $v<0$. To preclude the first possibility, one has to require that the maximum possible value of v occurring during the above cycle, $|v_{\max}|=2/\sqrt{3}$ remain within the multistability range. This restricts the value of the parameter $\alpha<\frac{1}{3}$. If all islands are of

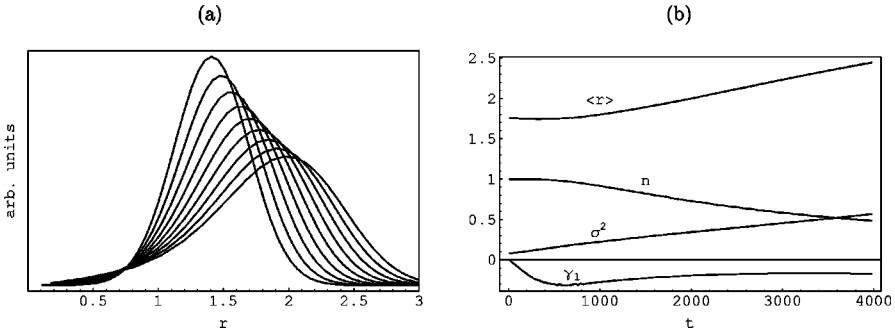

FIG. 2. (a) Snapshots of distributions evolving from an initial Gaussian distribution. The center of the distribution moves to the right and the profile becomes wider as time grows. The time step between successive profiles is $\Delta t = 95$. (b) Long-scale dynamics of the number of islands n, mean radius $\langle r \rangle$, dispersion σ^2, and skewness γ_1 of the island size distribution ($q = 2.43$, $K = 0.24$, $\alpha = 0.2$).

the same size, the minimum radius corresponding to $\eta = -b$ in Eq. (7) is $r_{\min} = \sqrt{n^{-1}(s - b/\beta)}$, which restricts the parameter $\beta > b/s$.

In an extended system ($L \gg 1$), Eq. (8) can still be retained as a dynamic equation of η, with local averaging understood as in Eq. (5). This typically leads, after a long evolution starting from random initial conditions, to the final state of a disordered spiral pattern.[11]

IV. RIPENING OF SURFACE PHASE DISTRIBUTION

The size distribution of islands of the minority phase evolves at long times due to a weak dependence of the velocity on curvature,

$$c = \delta\gamma[\psi(\alpha v) - \kappa\delta]. \tag{11}$$

For circular islands, $\kappa = r^{-1}$, and the dynamic equation for radii is

$$\frac{dr}{dt} \equiv c(v,r) = \delta\gamma\left[\psi(\alpha v) - \frac{\delta}{r}\right]. \tag{12}$$

The radii distribution necessary for evaluation of the surface area occupied by the minority phase in Eq. (7) obeys the first-order partial differential equation (PDE)

$$\frac{\partial f}{\partial t} + \frac{\partial (c(v,r) f)}{\partial r} = 0, \tag{13}$$

which has to be solved together with Eq. (6) where η is defined by Eq. (7). Since the velocity $c(v,r)$ changes sign during the oscillation cycle, Eq. (13) is ill-suited to a common finite-difference scheme of numerical integration but is readily solved by the method of characteristics. The characteristics are defined by Eq. (12); since $c(v,r)$ is a monotonic function of r, shocks are never formed, and the distribution is well behaved. Due to the variability of the velocity, the distribution function changes along the characteristic,

$$\frac{df}{dt} + f\frac{\partial c}{\partial r} = 0. \tag{14}$$

The ripening process should generally lead to slow elimination of smaller islands and growth of the average island size. This is accounted for in the computation by eliminating the islands when their radius falls below some critical value r_0, i.e., imposing a distribution cutoff.

Figure 1(b) shows the dynamics of the global variable v, the coverage fraction η, and the mean radius over the length of several periods. The form and period of oscillations changes slowly, in parallel with slow evolution of the island size distribution. Snapshots of distributions evolving from an initial Gaussian distribution and the long-time dynamics of statistical characteristics are shown in Fig. 2. To eliminate short-scale dynamics, all values are computed here at the lowest point of each oscillation cycle. Dispersion gradually increases, while the skewness becomes negative. Elimination of smaller islands becomes substantial after the lower tail of the distribution has reached the lower cutoff radius. Following this, the island number density decreases, the growth of the mean radius accelerates, and the trend of the evolution of the skewness reverses, reflecting preferential growth of larger islands. The total area occupied by the islands at the lowest point of each oscillation cycle (as at any other comparable phase of the cycle) remains constant to a high degree of accuracy. We expect therefore that the long-time distribution would follow the same Lifshitz–Slyozov formula[12] as in the classical equilibrium ripening process. These times are, however, irrelevant for our model since the islands size would reach at late stages of ripening the characteristic diffusion scale of the long-range variable, and the main postulate of the two-tier model would be violated.

V. BOUNDARY DYNAMICS

The presumption of a circular shape is well justified only when the interaction between islands is negligible. At higher densities of the minority phase, or, moreover, under conditions when the phases are interspersed and neither forms a connected continuum, the boundary dynamics is governed locally by Eq. (11) but the radius distribution is not well defined.

We have carried out detailed modeling of the ripening process with the help of a Lagrangian algorithm based on the local equation of boundary motion. Each island is represented by its boundary which, in turn, is approximated by a polygon, i.e., a directed array of points in the plane, which propagates according to Eq. (11) with the velocity dependent on the instantaneous value of v and the local curvature approximated by finite differences. The long-scale variable v is treated also in these computations as a global variable, and its dynamics is governed by Eq. (6), where η is expressed through the total instantaneous area of the islands. The computation algorithm includes updating the boundary, checking for intersections, computing the area, and updating the value of the global variable v.

The most difficult part of the Lagrangian numerical algorithm is related to a possible merger of islands, as well as a change of their topology. The latter occurs, for example, when two elongated arms of a horseshoe-shaped island merge creating a ring-like island which is not simply connected. In order to record such events, it is necessary to test intersections of island boundaries at each calculation step. For a large number of islands, the testing procedure may be very time-consuming. The following algorithm was applied therefore to reduce number of operations. At the first stage, we create rectangular bounding boxes for each island, and check whether they intersect, which is a necessary (but not sufficient) condition of intersection of the corresponding pair of islands. This selects ''suspicious'' pairs of islands. At the next stage, intersections of elementary segments comprising the polygonal boundaries are tested for the selected pairs of islands only. In addition, each island is checked for self-intersections.

After all intersections are detected, a new set of boundaries is produced by reconnection. To avoid uncertainties in redrawing the boundaries, the time step is always adjusted dynamically in such a way that no more than two intersections occur simultaneously. Boundary smoothing is carried out following reconnection to eliminate spurious short loops. Such loops are also likely to emerge when an island shrinks in the course of the ripening process. This is prevented by setting a minimal size below which the island is eliminated from the computational process.

The ripening process on a smooth surface leads to elimination of smaller islands, while the surviving islands approach the circular shape. The average radius $\langle r\rangle = 2S/P$ (where P is the total perimeter of the interphase boundary, and S is the area occupied by the minority phase) exhibits steady growth on the background of short-scale oscillations.

A representative simulation run has been carried out starting from the initial picture shown in Fig. 3(a). The ripening process on the smooth surface leads to a fast decrease of the islands number, as seen in Fig. 4(a). The right part of the same figure shows the evolution of the mean radii of individual islands defined through the area to perimeter ratio. The values at the lowest point of each oscillation cycle are plotted here to eliminate short-scale oscillations. In a typical ripening picture, the radii of individual mid-size islands first grow and then start to decrease after smaller islands are eliminated, and the former ''middle class'' is swept in the lower decals of the distribution. The islands interact here only through the level of the long-range variable v; since short-scale interactions distorting the islands shape are absent, the islands evolve to a circular shape, and their merger is highly improbable.

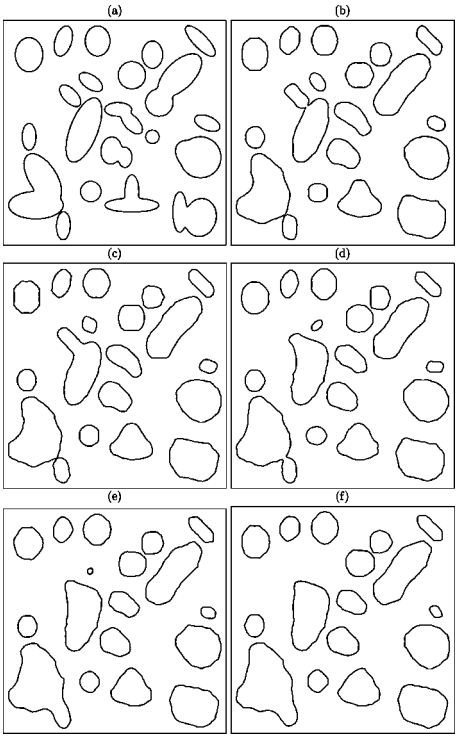

FIG. 3. The initial distribution (a) of islands used for numerical simulations of islands dynamics on flat and roughened surfaces, and snapshots of the successive distributions for $\Delta\rho = 0.7$ taken at (b) $t = 14$, (c) $t = 21$, (d) $t = 50$, (e) $t = 61$, and (f) $t = 75$.

VI. SURFACE ROUGHENING

The ripening can be suppressed on a rough surface. Self-induced roughening may be caused by surface modification taking place at locations traversed by the transition front between the alternate surface states. The surface modification may also compensate the ripening process by gradually lowering the upper limit of island growth during an oscillation cycle. It is reasonable to assume that surface roughening reduces the velocity of the boundary drift due to the change of the surface geometry.

We assume that the degree of surface roughening is a quasilocal property of the system and therefore can be modeled by its values at points of a two-dimensional grid with the grid step several times larger than the characteristic distance between polygon vertices approximating the interphase boundaries. When a boundary crosses a given grid point, the variable ρ describing the surface roughness at this point is increased by a certain prescribed value $\Delta\rho$. On the other hand, geometric inhomogeneities of the surface slowly attenuate with time due to thermal effects at the microscopic level. This process is described in our model by allowing for a continuous relaxation of the surface roughness following a linear equation $d\rho/dt = -\Gamma\rho$. The characteristic relaxation time Γ^{-1} must be much larger than a typical oscillation period of the macrovariable v.

Starting from an initially smooth surface, the swinging motion of island boundaries leads to a local increase of the surface roughness in the belts traversed in either direction. The increased roughness causes local deceleration of the boundary drift, which effectively freezes the ripening process. Slow relaxation of the roughness leads to a dynamical balance between the boundary motion and roughness dynamics. As a result, the system is left in a disordered state strongly dependent on initial conditions.

The computational algorithm allowing for surface modification is far more complex than that described in the preceding section, as it should combine Lagrangian boundary

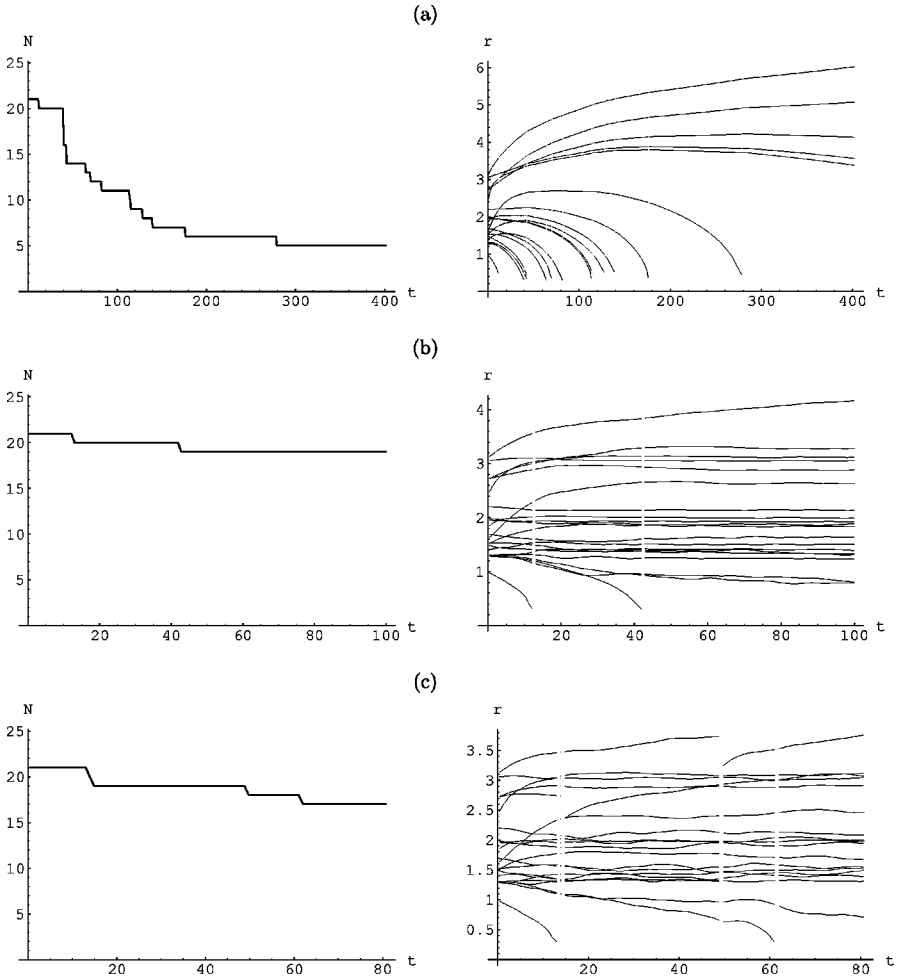

FIG. 4. The dynamics of the islands number and their mean radii for (a) smooth ($\Delta\rho=0$) and roughened (b) ($\Delta\rho=0.3$) and (c) ($\Delta\rho=0.7$) surfaces. The rougheness relaxation time is $1/\Gamma=0.1$. Vertical white strips mark the island elimination events.

dynamics with Eulerian evolution of local roughness. In addition to the subroutines of updating the boundaries and testing for boundary intersections, the combined algorithm includes searching for grid points crossed by the boundaries, and updating the roughness value at the grid points.

Each grid point P_{ij} of a square grid is assigned a binary tag taking the value $K_{ij}=1$ when the point is inside an island and $K_{ij}=0$ if it lies outside. The tag has to be switched whenever a given grid point is traversed by any boundary segment at each Lagrangian propagation step. A straightforward algorithm testing all possible tag switch events is very time-consuming and ineffective. A much faster algorithm is based on division of grid lines into a finite number of segments each containing points with the same value of the tag K. For example, a grid line with a fixed index $i=I$ crossing N island boundaries may be divided into $N+1$ segments: $j\in(1,j_1)\cup(j_2+1,j_3)\cup\ldots$ with $K_{I,j}=0$ and $j\in(j_1+1,j_2)\cup(j_3+1,j_4)\cup\ldots$ with $K_{I,j}=1$. It is sufficient then to trace only points with the indices $j=j_1+1,j_2,j_3+1,j_4,\ldots$ which bound the segments with $K=1$. We need to trace each boundary only once in order to determine the full set of such points. As a result, the computation time is roughly proportional to the length of the boundary, rather than to the total number of grid points, as when the naive algorithm is applied.

Figure 3 shows the initial distribution of islands used in simulations on both smooth and rough surface, and the snapshots of a few successive distributions in a simulation run starting from an originally smooth surface. The dynamics of islands number and of their mean radii for surfaces with two different roughening rates $\Delta\rho$ are shown in Figs. 4(b) and 4(c). It is clearly seen that the tendency to evolve to a circular shape, as well as elimination of smaller islands are suppressed as the surface roughness develops. The self-induced roughening thus freezes a state of spatial chaos initiated by the original distribution. At a larger roughening rate, the number of eliminated islands is very small, and the mean radii of the remaining islands remain effectively unchanged after the surface roughness develops.

VII. CONCLUSION

The two-tier model described above combines features found in the standard FitzHugh–Nagumo model at different ratios of characteristic relaxation times and diffusivities of the species involved. On the macroscopic level, v is a fast activator, while η plays the role of a nondiffusive slow inhibitor. At the same time, on the microscopic level, u is a slow short-range activator while v is a fast long-range inhibitor. This combination allows to generate oscillations and waves on the macroscopic level, and phase separation with slowly drifting interphase boundaries on the microscopic level. The two levels are related by the averaging procedure

defining the evolution equation of η. The physical origin of the averaging is in sampling of large surface areas by the diffusive macrovariable.

The distribution of surface phases ripens at long times due to preferential growth of larger islands. The ripening process may be arrested by surface inhomogeneities which develop dynamically as a result of slow surface modification and roughening.

In a wider perspective, interactions between chemical reactions and phase transitions can be seen as a powerful and still poorly explored source of spatio-temporal complexity. In this communication, we use different computational strategies at the two widely separated length scales characteristic to this system, combining Lagrangian computations of motion of interphase boundaries with usual Eulerian computations on a fixed grid with a wider spacing. This allows us to describe multiscale dynamics on a finer level of detail, and account for spontaneously developing inhomogeneities.

The model can be further elaborated accounting for effects of anisotropy, both on the microscopic and on the microscopic level. Different models of surface modification, alternative to the simple model discussed above, may be introduced. In particular, the roughened zones which have been often traversed by the interphase boundary, can be assigned special kinetic properties, which might model recently observed wave pulses propagating along the border between alternative surface states.[13] A still finer level of description should account for fluctuations, that may be resolved by molecular simulations of surface reconstruction.

ACKNOWLEDGMENTS

This research has been supported by the Ministry of Science and Arts of Niedersachsen. We thank Ronald Imbihl for numerous helpful discussions.

[1] M. Eiswirth and G. Ertl, in *Chemical Waves and Patterns*, edited by R. Kapral and K. Showalter (Kluwer, Dordrecht, 1994).
[2] R. Imbihl and G. Ertl, Chem. Rev. **95**, 697 (1995).
[3] R. Imbihl, M. P. Cox, G. Ertl, H. Müller, and W. Brenig, J. Chem. Phys. **83**, 1578 (1985).
[4] M. Eiswirth, P. Möller, K. Wetzl, R. Imbihl, and G. Ertl, J. Chem. Phys. **90**, 510 (1989).
[5] K. Krischer, M. Eiswirth, and G. Ertl, J. Chem. Phys. **96**, 9161 (1992).
[6] M. Bär, M. Hildebrand, M. Eiswirth, M. Falcke, H. Engel, and M. Neufeld, Chaos **4**, 499 (1994).
[7] S. Ladas, R. Imbihl, and G. Ertl, Surf. Sci. **197**, 153 (1988); **198**, 42 (1988).
[8] R. Imbihl, A. E. Reynolds, and D. Kaletta, Phys. Rev. Lett. **67**, 275 (1991).
[9] R. Imbihl, Mod. Phys. Lett. B **6**, 493 (1992).
[10] T. Gritsch, D. Coulman, R. J. Behm, and G. Ertl, Phys. Rev. Lett. **63**, 1086 (1989).
[11] L. M. Pismen, R. Imbihl, B. Y. Rubinstein, and M. I. Monin, Phys. Rev. E **58**, 2065 (1998).
[12] E. M. Litshitz and V. V. Slyozov, J. Phys. Chem. Solids **19**, 35 (1961).
[13] K. C. Rose, B. Berton, R. Imbihl, W. Engel, and A. M. Bradshaw, Phys. Rev. Lett. **79**, 3427 (1997).